

Electron-electron interaction in the ionization of O^{7+} by He

W. Wu,* K. L. Wong,[†] E. C. Montenegro,[‡] R. Ali,[§] C. Y. Chen, C. L. Cocke, R. Dörner,^{||} V. Frohne,[¶] J. P. Giese, V. Mergel,^{||} W. E. Meyerhof,** M. Raphaelian,^{††} H. Schmidt-Böcking,^{||} and B. Walch
J. R. Macdonald Laboratory, Physics Department, Kansas State University, Manhattan, Kansas 66506

(Received 19 August 1996)

Contributions of the electron-electron and electron-nucleus interactions to the ionization of O^{7+} by He are experimentally separated using recoil momentum spectroscopy. The electron-electron contribution is found to produce much smaller recoil momenta, both longitudinal and transverse. The momentum distributions of the two mechanisms are in good agreement with theoretical predictions. The comparison between the experiment and the theory suggests that electron-electron interactions in the projectile ionization can be understood in terms of free-electron impact ionization of the projectile ions. [S1050-2947(97)09702-3]

PACS number(s): 34.50.Fa, 34.80.Dp

I. INTRODUCTION

The ionization of a hydrogenlike projectile by a He target can be driven by two different interactions. The first is the interaction between the projectile electron and the screened He nucleus (eN interaction), and the second one is between the projectile electron and target electrons (ee interaction) [1–6]. The eN interaction is understood here as the interaction with the screened target, which is left in its ground state after collision, and implicitly includes some projectile-electron–target-electron interaction (screening). Generally, this is the more important process, which is historically more thoroughly studied. In the ee interaction, the target electrons act as quasifree electrons and obey kinematic conditions appropriate to the interaction of nearly free electrons with the projectile.

While the importance of the ee interaction has been theoretically recognized within the Born approximation since 1953 [1], experimental evidence was not seen until 1989 [7]. The ee process has a threshold at an ion velocity approximately equal to the threshold electron velocity in the corresponding free-electron impact ionization. The “approximation” in the ion-atom case is caused by the motion of the target electron in the target nuclear potential. Hülskötter

et al. [7] reported enhancements in the ionization cross section for C^{5+} and O^{7+} in collisions with He and H_2 above this threshold velocity, and showed that the excess of the cross section above what one would expect for the eN ionization could be attributed to the ee contribution. Further evidence for the ee process was observed by Montenegro *et al.* [8] in the ionization of He^+ by He and H_2 at high velocities where the ee mechanism dominates.

A clear separation of the ee and eN processes relies on differential cross-section measurements. Montenegro *et al.* [9] reported evidence for the influence of the ee interaction in the scattering angle (projectile transverse momentum) dependence for the ionization of C^{5+} and O^{7+} by He and H_2 . More recently, the ee and eN processes were completely separated by Dörner *et al.* [10] and Wu *et al.* [11] by measuring the recoil longitudinal momentum transfer. The basic physics for the separation of the two mechanisms is that the eN interaction throws the recoil He ion forward while the ee interaction leaves it nearly at rest. The momentum and energy transferred to the projectile electron in the eN interaction are supplied by the He atom acting coherently as a whole. Conservation of momentum and energy leads to the result that the He recoil is thrown forwards with a longitudinal momentum P_z given by Q/v for small-angle scatterings [10,11]. Here v is the projectile velocity and Q is the magnitude of the electronic energy that the projectile must receive to be ionized, i.e., the sum of the binding energy of the projectile electron plus the kinetic energy of the ionized electron in the projectile frame. On the other hand, when the projectile is ionized by interacting with a quasifree He electron, the remaining He^+ ion core is just a spectator to the process and is left with only its original small Compton momentum. Thus the ee process should leave the recoil nearly at rest.

The possible reaction channels and the corresponding interactions are illustrated in Fig. 1. While the ee process produces a He^+ ion, the eN process will leave a neutral He unless some other interaction also ionizes the He atom during the same collision. If this interaction is that between the projectile nucleus and one of the He electrons, it would be described within a Born approximation formalism as a second-order process. In the present experiment, since the projectile charge is large and the projectile must pass very

*Present address: Lawrence Berkeley National Laboratory, 1 Cyclotron Road, MS 88-103, Berkeley, CA 94720.

[†]Present address: Lawrence Livermore National Laboratory, P.O. Box 808, L-43, Livermore, CA 94550.

[‡]Permanent address: Departamento de Física, Pontifícia Universidade Católica do Rio de Janeiro, Caixa Postal 38071, Rio de Janeiro, RJ 22452, Brazil.

[§]Present address: Department of Physics, University of Nevada-Reno, Reno, NV 89557.

^{||}Permanent address: Institut für Kernphysik, Universität Frankfurt, 60486, Frankfurt, Germany.

[¶]Present address: Physics Department, Western Illinois University, Macomb, IL 61455.

**Permanent address: Physics Department, Stanford University, Stanford, CA 94305.

^{††}Present address: ALCEDO, 1050 Stewart Drive, Sunnyvale, CA 94086.

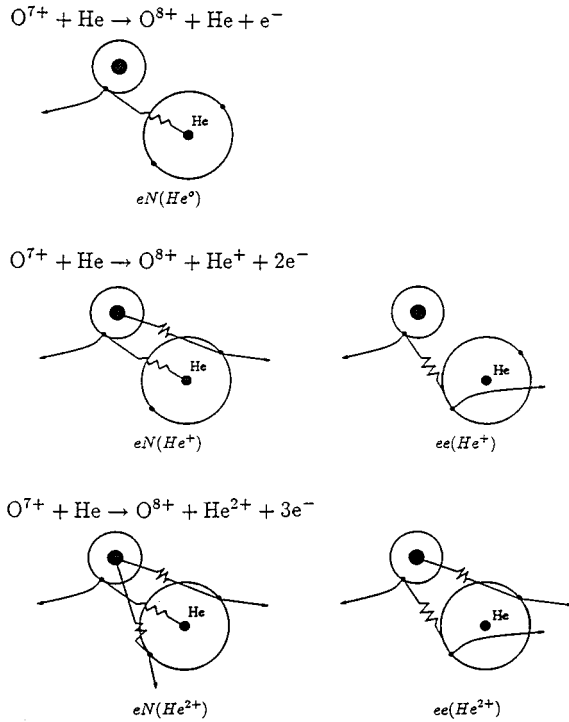


FIG. 1. Illustration of reaction channels and possible processes that contribute to the ionization of O^{7+} by He.

close to the He nucleus in order to be ionized, the ionization of He by the projectile is a very probable process in the intermediate velocity region. As the projectile energy increases, the relative importance of these high-order mechanisms decreases [8,10].

In this work we report momentum distributions for ee and eN processes up to a bombarding energy of 75 MeV, where the contribution from the ee process becomes more pronounced. We further provide quantitative analyses of these distributions in both transverse and longitudinal momentum.

II. EXPERIMENT

The experiment was carried out in the J. R. Macdonald laboratory at KSU. O^{7+} beams of 20–40 MeV were obtained directly from the Tandem Van de Graaff accelerator, and higher-energy O^{7+} ions were obtained by further acceleration through the LINAC. The experimental apparatus and technique have already been described in detail elsewhere [12]. Briefly, the projectile ions passed through a target He jet collimated so that the thermal momentum of the target along the beam direction was limited to approximately 0.6 a.u. He ions produced in the collision region were extracted at right angles to the beam by an electric field of 5 V/cm and sent onto a position-sensitive channelplate detector. The projectiles were charge-state analyzed and detected by a second position-sensitive channelplate detector located 4 m downstream. The major charge-state selection was accomplished by magnets located 0.5 m before and after the collision region. Additional charge-state selection was provided by two electrostatic deflectors, with opposite polarity, positioned 0.05 m before and after the jet and deflecting in the plane normal to that of the magnetic deflection. Corrections for

events due to double collisions and random coincidences are important for this experiment because the cross section for target ionization is about 2 orders of magnitude larger than that for projectile ionization. These corrections were made possible by using our rather complete magnetic and electrostatic charge analysis system to isolate double collision contributions. The main beam was prevented from reaching the projectile detector by a beam block so that only projectile ions that had lost one electron were detected. The flight time between the detection of the projectile and the recoil, and the position at which the recoil hit on the recoil detector, were used to determine the recoil charge state and all three components of its vector momentum [12].

III. RESULTS AND DISCUSSION

A. Longitudinal momentum distributions

Recoil longitudinal momentum (p_z) distributions for projectile ionization accompanied by target single ionization (He^+) and double ionization (He^{2+}) are shown in Fig. 2. They are plotted in Q -value space ($Q = p_z v$) so that positions corresponding to ionization of an electron from the projectile into a particular continuum state are aligned for different projectile energies. The ee threshold energy for the O^{7+} system is 26 MeV, and the He^+ data reveal the growth of a second peak attributable to this process near $p_z = 0$ ($Q = 0$) for projectile energies above this energy. The feature is less pronounced in the He^{2+} channel. The experimental resolution in p_z was measured to be 0.6 a.u. [full width at half maximum (FWHM)] [12]. The broader peak widths seen for both the ee and eN mechanisms are caused by target ionization that involves the electrons in the target continuum. Such broadening is expected to be broader for the He^{2+} channel than for the He^+ channel because the former involves one more electron in the target continuum. This partially explains why the separation between the ee and eN mechanism is less pronounced when a He^{2+} is produced. At higher collision energies where the ee contribution overtakes the eN contributions, a clear ee distribution near $Q = 0$ emerges in the He^{2+} channel.

We now suggest quantitative models for the description of those spectra of Fig. 2 in which He^+ is produced. If the projectile is ionized by the eN interaction, this eN channel will be hereafter referred to as loss ionization [LI, Fig. 1, $eN(He^+)$]. Within the independent electron approximation formalism, LI can be described as projectile ionization due to the screened He nucleus, accompanied by the target ionization via interaction between the projectile nucleus and one of the target electrons. The eN process for projectile ionization is caused by interaction of the projectile with the screened He nucleus [13,14], but the screening is nearly negligible in this case because the O^{7+} can only be ionized for impact parameters well inside the He screening radius. Neglecting this screening, we thus carried out a SCA (semiclassical approximation) calculation [15] in the projectile frame using an unscreened He nucleus. The resulting differential cross section is shown in Fig. 3 as a solid line for the collision energy of 20 MeV, where the total cross section has been normalized to 1. The threshold at $Q = 32$ a.u. is the ionization potential of O^{7+} .

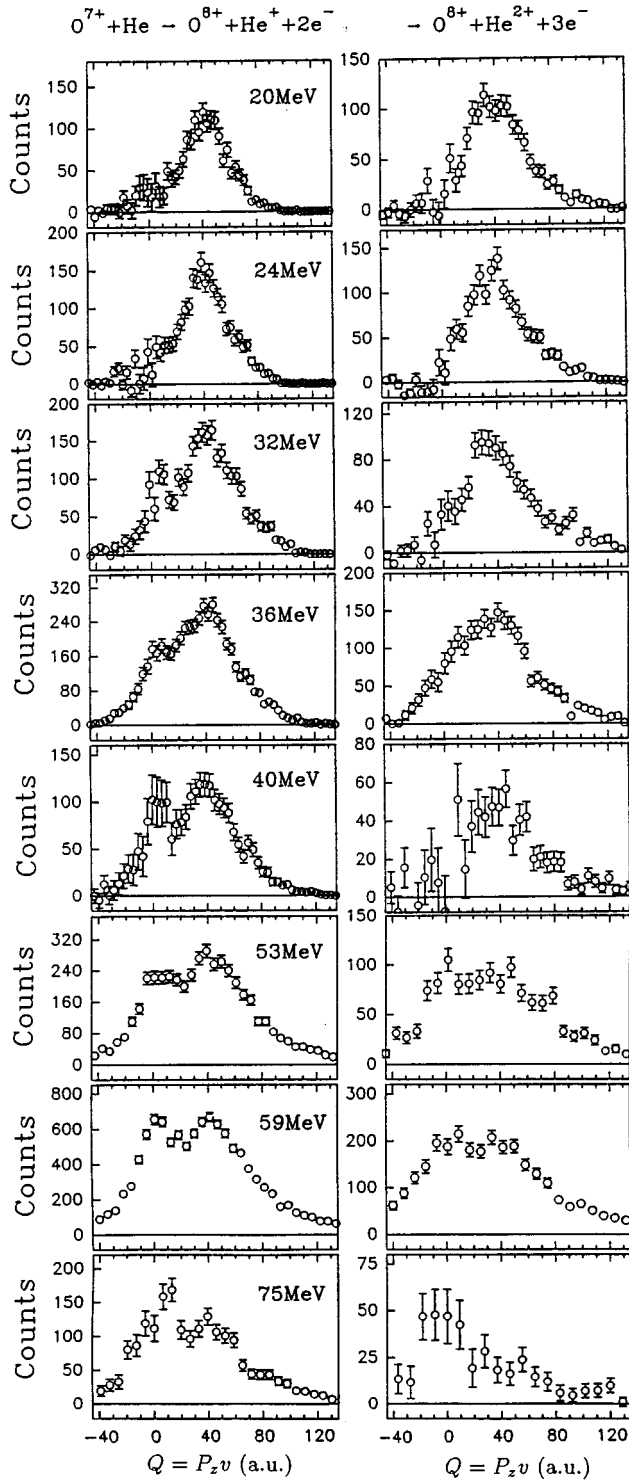


FIG. 2. Longitudinal recoil momentum spectra for O^{7+} on He. $Q = P_z v$ is the endoergicity of the collision if the projectile electron energy is measured in the projectile frame.

The spectrum calculated above should reflect the momentum distribution of a neutral He recoil, not that of the recoiling He^+ ion. Thus an additional broadening of the Q spectrum of Fig. 2 due to the momentum carried away by the target electron must be included. We have taken this into account by assuming that the experimental p_z distribution for target single ionization (where the projectile remains unchanged) is the same as that for target single ionization ac-

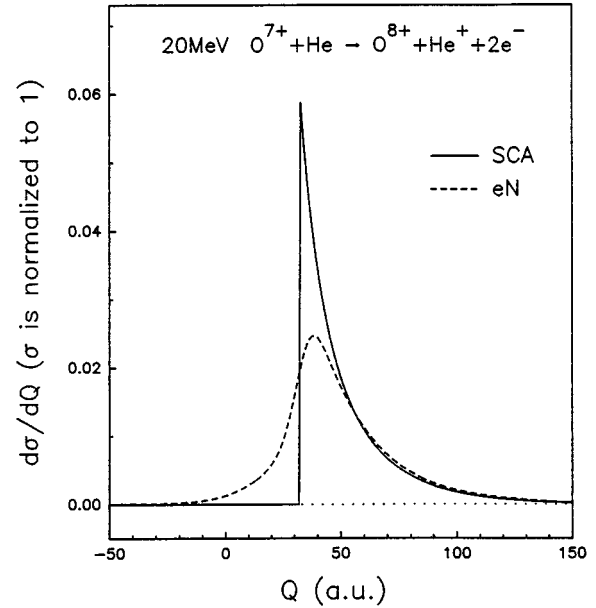


FIG. 3. Model spectra for the ionization of 20-MeV O^{7+} via the eN process. The solid line is an SCA calculation for projectile ionization only, and the dashed line is the model spectrum for projectile ionization accompanied by He^+ recoils.

companied by projectile ionization. This experimental p_z distribution was measured by recording He^+ recoil position in coincidence with the primary beam (O^{7+}) [12]. The result obtained by folding the SCA spectrum of Fig. 3 into the target ionization p_z distribution is shown in Fig. 3 as a dashed line. There may be a slight difference between the distributions for target ionization accompanied by projectile ionization and pure single target ionization because they may occur at different impact parameters. Dörner *et al.* [16] have shown that for single ionization in $H^+ + He$ collisions, the p_z distribution becomes broader at smaller impact parameters. One estimate of the momentum distribution for target ionization accompanied by projectile ionization from first principles is, however, not practically feasible at the moment.

If the projectile ionization accompanied by He^+ production is caused by the ee mechanism, no further interaction is needed [Fig. 1, $ee(He^+)$]. The recoil He^+ for this mechanism can be treated as a spectator. The measured recoil p_z is then due to the Compton profile of the target, i.e., $p_z = -p_z^e$, where p_z^e is the longitudinal momentum of the target electron when it is interacting with the projectile electron. The p_z differential cross section due to the ee process can be written in the impulse approximation as [17]

$$\frac{d\sigma_{ee}(He^+)}{dp_z} = \sigma_{\text{eff}}[E_e(p_z^e)]J(p_z^e) = \sigma_{\text{eff}}[E_e(-p_z)]J(-p_z), \quad (1)$$

where $\sigma_{\text{eff}}(E_e)$ is the cross section for the ionization of the projectile by a free electron with energy E_e , and $J(p_z^e)$ is the density of target electron at a momentum p_z^e , which is associated with the target Compton profile. The kinetic energy E_e for the target electron in the projectile frame can be written from energy conservation considerations as (in atomic units) [18]

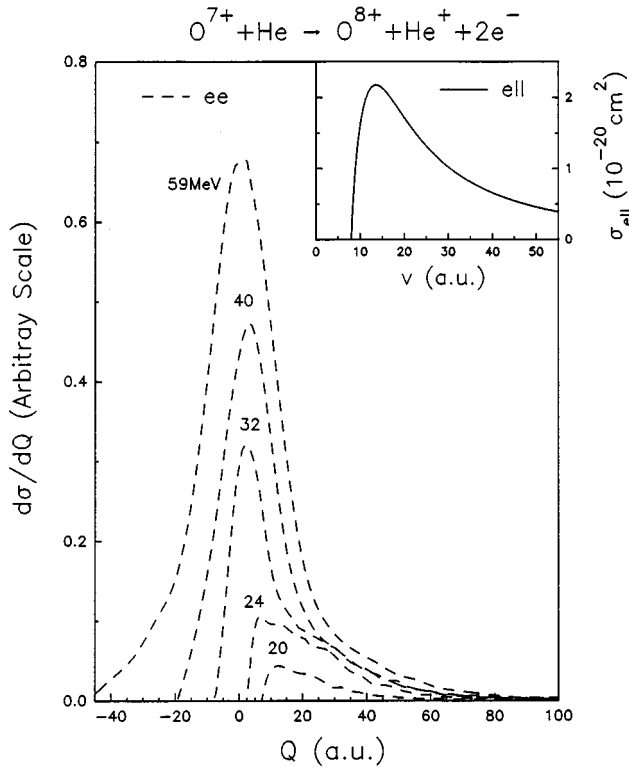


FIG. 4. Model spectra for the ee mechanism of the ionization of O^{7+} at different collision energies. The inset is the CBE calculation for free-electron impact ionization (eII) of O^{7+} . Waves seen for the 20- and 24-MeV data are due to the statistics of the experiment distribution, which is folded into the model (see text).

$$\begin{aligned}
 E_e &\approx \frac{1}{2}(-v)^2 + (-v)(p_z^e) - I_{He} \\
 &= \frac{1}{2}(-v)^2 + (-v)(-p_z) - I_{He}, \quad (2)
 \end{aligned}$$

where I_{He} is the ionization potential of He, v is the velocity of the projectile, and $-v$ is the velocity of the target in the projectile frame. The signs for the velocity and momentum are retained in the equation to show that a target electron moving towards the projectile has bigger kinetic energy in the projectile frame than an electron initially moving in the opposite direction. The electron impact ionization cross section σ_{eII} was calculated from the Coulomb-Born-exchange (CBE) model [19]. We used the experimental distribution for target single ionization as $J(P_z)$, since this is expected to be close to the results of folding the Compton profile with the experimental resolution function in this case. The resulting differential cross section for the ee interaction is shown in Fig. 4, where P_z has been converted to Q following $Q = P_z v$. The important feature of this model is that the peak position for the ee process is shifted towards positive Q by an amount that decreases with increasing projectile energy. This is consistent with the experimental spectra shown in Fig. 2. The reason for this is the strong onset of σ_{eII} at velocities near the threshold (Fig. 4 inset). Thus, a target electron moving towards the projectile has a bigger cross section than a target electron moving away from the projectile. For 20- and 40-MeV projectiles, whose velocities are below the threshold for electron impact ionization of O^{7+} , only positive P_z val-

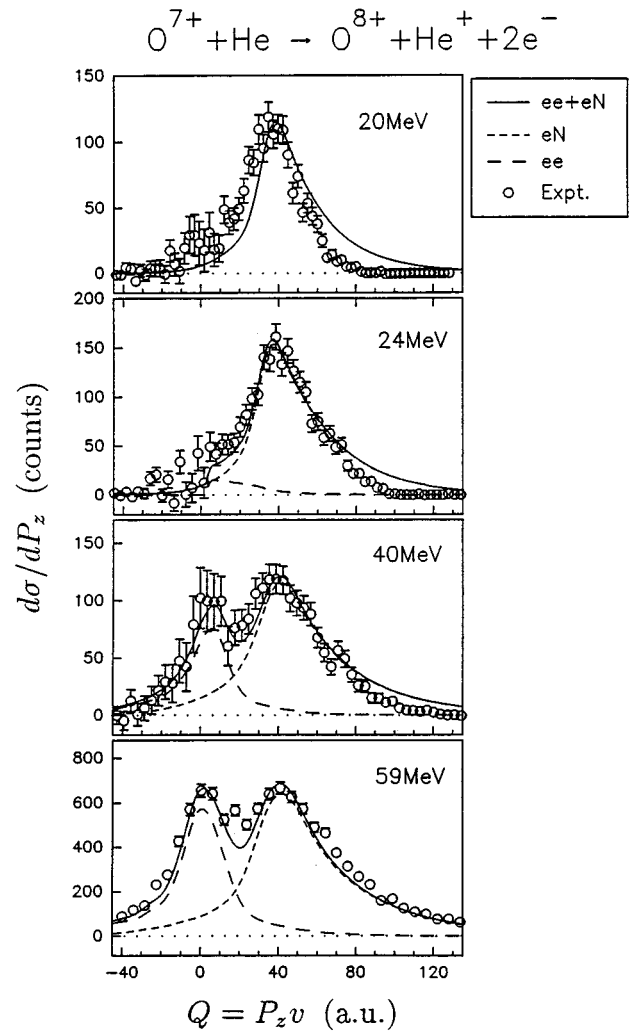


FIG. 5. Longitudinal recoil momentum spectra for ionization of O^{7+} in coincidence with a He^+ . Dashed lines are from the models spectra for the eN process (short dashed line) and the ee process (long dashed line). Solid lines are fits to the present data obtained by adjusting the ee/eN ratio.

ues, corresponding to target electrons with velocity larger than threshold velocity in the projectile frame, contribute.

The final model distributions for the eN and ee processes were compared to the experiment by adjusting the ee/eN cross section ratio so that the model fit the experimental distribution visually. The results are shown in Fig. 5. The overall theoretical distribution for each spectrum was normalized to the experiment. The agreement in shape between the experiment and the model is very good. The shape for the ee distribution is well accounted by the theory, while the agreement for the eN shape is not as good as that for the ee part. The results indicate that the SCA is a good approximation for the eN process, and the ee process can be understood in terms of the free-electron impact ionization of the projectile, modulated by the target Compton profile. The conclusion is a step beyond our earlier analysis on total ee and eN cross sections [11,20], where we showed that the contribution of the ee interaction relative to the total eN process was in good agreement with the plane-wave Born approximation and impulse approximation calculations [11], and that the total cross section for the ee process was nearly

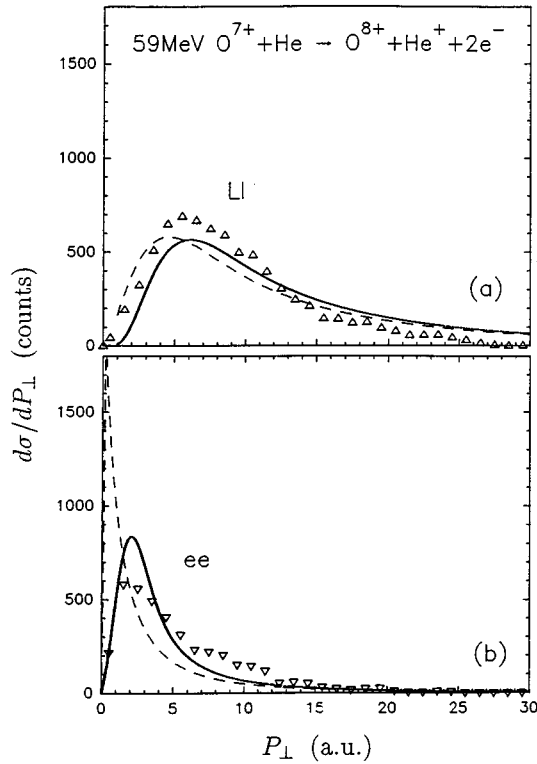


FIG. 6. Transverse recoil momentum spectra for ionization of O^{7+} in coincidence with a He^{+} caused by (a) two-electron–nucleus interactions, loss-ionization (LI), and (b) one single ee interaction (ee). Dashed lines are the model distributions, and solid lines are the model distributions convoluted with the experimental resolution (see text).

identical to the corresponding cross section for free-electron impact ionization [20].

B. Transverse momentum distributions

In Ref. [11], we showed that the ee interaction can be separated from the eN process in the two-dimensional recoil longitudinal-transverse momentum spectra. This allows us to isolate the transverse momentum (p_{\perp}) distributions, and to obtain the impact parameter dependence for the ee and eN interactions separately. Here we present and analyze those separately. The p_{\perp} distribution for the ionization of 59-MeV O^{7+} accompanied by He^{+} is plotted in Fig. 6, where (a) is for the (LI) process caused by two electron-nuclear interactions, and (b) is for the process due to a single ee interaction. The comparison shows that the ee process peaks at smaller p_{\perp} than the eN process, indicating that the ee process is important at relatively larger impact parameters. The explanation is the following.

The LI process can be considered as a product of two electron-nucleus ionizations [Fig. 1, $eN(\text{He}^{+})$]. Following an independent electron description, the impact parameter (b) dependence of the LI probability, $P_{\text{LI}}(b)$, can be expressed as

$$P_{\text{LI}}(b) = 2P_i(b)[1 - P_i(b)]P_{eN}(b), \quad (3)$$

where $P_i(b)$ is the probability for ionizing the He by the projectile and $P_{eN}(b)$ is the probability for ionizing the pro-

jectile through the eN interaction. Because the projectile electron is much more tightly confined than the target electron, it is unlikely that $P_i(b)$ varies much over the range of impact parameters where $P_{eN}(b)$ is important. Thus $P_{\text{LI}}(b)$ can be simplified by using an impact parameter averaged probability (\overline{P}_i) for target ionization, $P_{\text{LI}}(b) \approx 2\overline{P}_i(1 - \overline{P}_i)P_{eN}(b)$. Within this approximation, the shape of the LI probability distribution is the same as the eN contribution to the projectile ionization. The same nonscreened target potential used for longitudinal momentum analysis in Sec. III A was assumed and $P_{eN}(b)$ was calculated within the SCA approximation [6].

The ee process is the incoherent ionization of the projectile by the target electrons [13,14]. The probability for this process to occur can be written as an SCA ionization probability, which is a function of the impact parameter between projectile nucleus and the various parts of the target electron cloud [5,6]. To obtain this probability as a function of the impact parameter relative to the target nucleus, i.e., b , we folded the former probability with the square of the target wave function. The result is that this process can occur at quite large b . The broader range of impact parameters where the ee interaction is effective, compared to the eN contribution, is indeed an important signature of the ee mechanism. Previous measurements by Montenegro *et al.* [9] indicated the preponderance of the ee over the eN contribution at large impact parameters. However, in order to have experimental access to the shape of the ee distribution, it would be necessary to measure projectile scattering angles smaller than 10^{-2} mrad, which was not possible with the experimental arrangement used in Ref. [9]. With the present measurements of the transverse recoil momentum, we are able to measure the impact parameter distribution corresponding to projectile scattering angles as low as 10^{-3} mrad, allowing a more direct comparison with the theoretical calculations.

The next question to be considered concerns the connection between the measured differential cross section $d\sigma/dp_{\perp}$ and the theoretical distribution $bP(b)$. Both LI and ee processes are four-body collision processes with two electrons left in the continuum after the collision (cf. Fig. 1). Thus, in principle, the transverse momentum balance among the He^{+} recoil, the projectile, and the two electrons has too many degrees of freedom to give a simple relation between the impact parameter b and the transverse momentum P_{\perp} . However, early studies of the recoil transverse momentum distribution for various systems such as $\text{U}^{32,65+} + \text{Ne}$ [21], $\text{F}^{9+} + \text{He}$ [22], and $\text{H}^{+} + \text{He}$ [16,23,24] suggest that, although there is no unique relation between P_{\perp} and b , the transverse recoil momentum is more closely related to the impact parameter than is the projectile scattering angle. We follow the analysis of [22] in which a ‘‘frozen-electron’’ model was developed. In this model, the relationship between b and p_{\perp} is obtained assuming that the role of the target electrons in determining the momentum exchange between the two interacting nuclei is to screen the nuclear field of the recoil nucleus. Under this assumption, the relationship between b and p_{\perp} , $p_{\perp}(b)$ can be obtained using a Bohr-like potential $V_{pt} = Z_p Z_t e^{-\beta R}/R$, where p and t refer to the projectile and target, respectively, $\beta = 2.206$ a.u. is the screening constant characterizing a bare projectile nucleus interacting with a neutral He atom, and R is the internuclear distance [22].

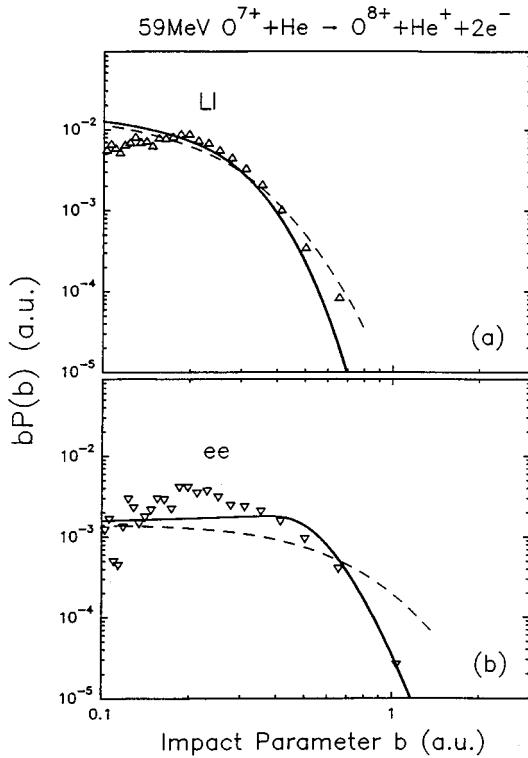


FIG. 7. Impact-parameter-dependent probabilities for the loss-ionization (LI) process (a) and the ee process (b). Dashed lines are the model distributions, and solid lines are the model distributions convoluted with the experimental resolution (see text).

Knowing the deflection function $p_{\perp}(b)$, the impact parameter probabilities can be obtained by the relation

$$bP(b) = \frac{1}{2\pi} \frac{d\sigma}{db} = \frac{1}{2\pi} \left| \frac{dp_{\perp}(b)}{db} \right| \frac{d\sigma}{dp_{\perp}}. \quad (4)$$

The experimental probability $P(b)$ obtained from Eq. (4) has a built-in experimental resolution. To make a proper comparison, the theoretical calculations must be convoluted with the experimental resolution distribution. Assuming that the x and y components of the transverse momentum, p_x and p_y , have a Gaussian resolution distribution with the same variance Γ , the resolution distribution for the transverse momentum $p_{\perp} = \sqrt{p_x^2 + p_y^2}$ is given by the Rayleigh distribution [25] $\mathfrak{R}(p_{\perp}) = (p_{\perp}/\Gamma^2) e^{-p_{\perp}^2/2\Gamma^2}$. The theoretical probability $P(b)$ was transformed into the p_{\perp} space using Eq. (4), convoluted with the Rayleigh distribution, and transformed back into b space. In the present measurements, $\Gamma = 0.85$ a.u., corresponding to a p_{\perp} width of 2.0 a.u. (FWHM).

Figures 6 and 7 show the recoil transverse momentum and the impact parameter differential cross sections for the LI and ee processes in 59-MeV $O^{7+} + He$ collisions. The normalization is such that in Fig. 6 the theoretical curves give the total number of experimental counts, and in Fig. 7 the experimental points give the total theoretical cross section. It can be seen from Fig. 7 that good agreement is obtained between the model calculations described above and the experimental data transformed into b space. The main features

described in the beginning of this section also clearly appear in these figures. At $b \sim 0$ the ee probability is about 10% of the LI due to the nonlocalized nature of the He electron cloud. Essentially for the same reason, the ee probability is more than an order of magnitude larger than the LI one at $b \sim 1$ a.u., showing clearly a flatter distribution.

On a linear scale, the broader impact parameter distribution of the ee process results in a sharply peaked model distribution near $p_{\perp} \sim 0$, as the dashed curve in Fig. 6(b) shows. For large impact parameters and small p_{\perp} , our transformation of p_{\perp} into b , which includes only the nuclear-nuclear repulsion, is only an approximation, both because it is not correct here to associate p_{\perp} with a classical b and because the transverse momentum imparted to the He atom can depart substantially from that finally carried off by the He^{+} ion. The observed shape for the ee process in the present experiment is, however, largely due to the experimental resolution, which hides to a considerable extent these shortcomings of the model for the ee process (cf. the solid line, which is the model distribution convoluted with the experimental resolution). The LI distribution, on the other hand, is not so much affected by the experimental resolution because large p_{\perp} is involved. This feature is common to mechanisms dominated by close collisions [22].

IV. CONCLUSION

In summary, the importance and the main dynamical features of the electron-electron interactions in ion-atom collision have been investigated for projectile ionization using recoil momentum spectroscopy. The contributions to the ionization of O^{7+} by the nucleus and the electrons of a He target were experimentally separated. The electron-electron contribution was found to produce much smaller recoil momentum, longitudinal and transverse to the beam direction. We have presented quantitative models that account for the longitudinal and transverse recoil momentum distributions for the projectile ionization accompanied by a He^{+} recoil. This channel can be reached by two-electron-nucleus interactions or by a single electron-electron interaction. For the eN contribution, comparisons between the model and the experiment show that the ionization of O^{7+} by He is very perturbative and the semiclassical calculations explain the major feature of the eN distributions, both longitudinal and transverse. For the ee contribution, a model based on the impulse approximation reproduces the experimental recoil longitudinal momentum distributions very well, indicating that the ee process can be understood in terms of free-electron impact ionization of the projectile, modulated by the target Compton profile. A full understanding of the recoil transverse momentum distribution for ee process is limited by the experimental resolution, but its main signature, i.e., its broad distribution in the impact parameter space, is clearly identified.

ACKNOWLEDGMENTS

We would like to thank K. D. Carnes, T. J. Gray, and V. Needham for providing the LINAC beams, and D. Trautmann and F. Rösler for making their SCA code available to

us. This work was supported by the Division of Chemical Sciences, Office of Basic Energy Sciences, Office of Energy Research, U.S. Department of Energy. E.C.M. was supported in part by CNPq (Brazil). R.D. and V.M. wish to acknowl-

edge the support of the Max Planck Forschungspreis of the Humboldt foundation and of the DFG, which made the visit to KSU possible. W.E.M. was partially supported by NSF Grants No. INT-9013087 and No. PHY-9019293.

-
- [1] D. R. Bates and G. Griffing, Proc. Phys. Soc. London Sect. A **66**, 961 (1953); **67**, 663 (1954); **68**, 90 (1955).
- [2] J. H. McGuire, N. Stolterfoht, and P. R. Simony, Phys. Rev. A **24**, 97 (1981).
- [3] R. Anholt, Phys. Lett. **114A**, 126 (1986).
- [4] E. C. Montenegro, G. M. Sigaud, and W. E. Meyerhof, Phys. Rev. A **45**, 1575 (1992).
- [5] E. C. Montenegro and W. E. Meyerhof, Phys. Rev. A **46**, 5506 (1992).
- [6] E. C. Montenegro, W. E. Meyerhof, and J. H. McGuire, Adv. At. Mol. Phys. **34**, 249 (1994).
- [7] H.-P. Hülskötter, W. E. Meyerhof, E. Dillard, and N. Guardala, Phys. Rev. Lett. **63**, 1938 (1989); H.-P. Hülskötter, B. Feinberg, W. E. Meyerhof, A. Belkacem, J. R. Alonso, L. Blumenfeld, E. Dillard, H. Gould, N. Guardala, G. F. Krebs, M. A. McMahan, M. E. Rhoades-Brown, B. S. Rude, J. Schweppe, D. W. Spooner, K. Street, P. Thieberger, and H. E. Wegner, Phys. Rev. A **44**, 1712 (1991).
- [8] E. C. Montenegro, W. S. Melo, W. E. Meyerhof, and A. G. de Pinho, Phys. Rev. Lett. **69**, 3033 (1992).
- [9] E. C. Montenegro, A. Belkacem, D. W. Spooner, W. E. Meyerhof, and M. B. Shah, Phys. Rev. A **47**, 1045 (1993).
- [10] R. Dörner, V. Mergel, R. Ali, U. Buck, C. L. Cocke, K. Froschauer, O. Jagutzki, S. Lencinas, W. E. Meyerhof, S. Nüttgens, R. E. Olson, H. Schmidt-Böcking, L. Spielberger, K. Tökesi, J. Ullrich, M. Unverzagt, and W. Wu, Phys. Rev. Lett. **72**, 3166 (1994).
- [11] W. Wu, K. L. Wong, R. Ali, C. L. Cocke, V. Frohne, J. P. Giese, M. Raphaelian, B. Walch, R. Dörner, V. Mergel, H. Schmidt-Böcking, and W. E. Meyerhof, Phys. Rev. Lett. **72**, 3170 (1994).
- [12] W. Wu, K. L. Wong, C. L. Cocke, J. P. Giese, and E. C. Montenegro, Phys. Rev. A **51**, 3718 (1995).
- [13] E. C. Montenegro and W. E. Meyerhof, in *Two-Center Effects in Ion-Atom Collisions*, edited by T. J. Gay and A. F. Starace, AIP Conf. Proc. No. 362 (AIP, New York, 1996), p. 103.
- [14] J. Wang, J. H. McGuire, and E. C. Montenegro, Phys. Rev. A **51**, 504 (1995).
- [15] The SCA calculation method used is described by M. Pauli and D. Trautmann in J. Phys. B **11**, 667 (1978), and M. Pauli, F. Rösel, and D. Trautmann in J. Phys. B **11**, 2511 (1978). The calculation for this case was carried out by using the "IONHYD" code provided by D. Trautmann.
- [16] R. Dörner, V. Mergel, Z. Liu, J. Ullrich, L. Spielberger, and H. Schmidt-Böcking, J. Phys. B **28**, 435 (1995).
- [17] E. C. Montenegro, W. Wu, K. L. Wong, and C. L. Cocke, Nucl. Instrum. Methods Phys. Res. B **99**, 62 (1995).
- [18] D. H. Lee, T. J. M. Zouros, J. M. Sanders, P. Richard, J. M. Anthony, Y. D. Wang, and J. H. McGuire, Phys. Rev. A **46**, 1374 (1992).
- [19] D. L. Moore, L. B. Golden, and D. H. Sampson, J. Phys. B **13**, 385 (1980).
- [20] C. L. Cocke and E. C. Montenegro, Comments At. Mol. Phys. **32**, 131 (1996).
- [21] J. Ullrich, R. E. Olson, R. Dörner, V. Dangendorf, S. Kelbch, H. Berg, and H. Schmidt-Böcking, J. Phys. B **22**, 627 (1989); R. E. Olson, J. Ullrich, and H. Schmidt-Böcking, Phys. Rev. A **39**, 5572 (1989).
- [22] K. Wong, W. Wu, E. C. Montenegro, I. Ben-Itzhak, C. L. Cocke, J. P. Giese, and P. Richard, J. Phys. B **29**, L209 (1996).
- [23] R. Dörner, J. Ullrich, H. Schmidt-Böcking, and R. E. Olson, Phys. Rev. Lett. **63**, 147 (1989); R. Dörner, J. Ullrich, O. Jagutzki, S. Lencinas, H. Schmidt-Böcking, and R. E. Olson, Z. Phys. D **21**, 57 (1991).
- [24] M. Horbatsch, J. Phys. B **22**, L639 (1989).
- [25] R. G. Brown, *Introduction to Random Signal Analysis and Kalman Filtering* (Wiley, New York, 1983).